Gene Therapy (2023) 30:64–74
https://doi.org/10.1038/s41434-021-00256-8

ARTICLE

Oncolytic Newcastle disease virus expressing the co-stimulator OX40L as immunopotentiator for colorectal cancer therapy

Limin Tian[1] · Tianyan Liu[2] · Shan Jiang[2] · Yukai Cao[1] · Kai Kang[1] · Han Su[1] · Guiping Ren[1] · Zhenzhong Wang[2] · Wei Xiao[2] · Deshan Li[1,3]

Received: 26 October 2020 / Revised: 2 March 2021 / Accepted: 26 March 2021 / Published online: 4 October 2021

Abstract

NDV as an attractive candidate for oncolytic immunotherapy selectively lyses tumor cells but shows limited anti-tumor immunity. Immune co-stimulator OX40 ligand (OX40L) boosts anti-tumor immunity response by delivering a potent costimulatory signal to $CD4^+$ and $CD8^+$ T cells. To improve the anti-tumor immunity of NDV, the recombinant NDV expressing the murine OX40L (rNDV-mOX40L) was engineered. The viral growth kinetics was examined in CT26 cell lines. The ability of rNDV-mOX40L to express mOX40L was detected in the infected tumor cells and tumor tissues. The anti-tumor activity of rNDV-mOX40L was studied in the CT26 animal model. Tumor-specific $CD4^+$, $CD8^+$ and $OX40^+$ T cells were examined by immunohistochemistry staining. The virus growth curve showed that the insertion of the mOX40L gene did not affect the growth kinetics of NDV. rNDV-mOX40L expresses mOX40L and effectively inhibits the growth of CT26 colorectal cancer in vivo. The tumor inhibition rate of the rNDV-mOX40L-treated group was increased by 15.8% compared to that of NDV-treated group in the CT26 model. Furthermore, immunohistochemistry staining of tumor tissues removed from the CT26 model revealed that intense infiltration of tumor-specific $CD4^+$, $CD8^+$ T cells, especially $OX40^+$ T cells were found in the rNDV-mOX40L-treated group. FACS showed that rNDV-mOX40L significantly enhanced the number of $CD4^+$ and $CD8^+$ T cells in spleen. Moreover, compared to the NDV-treated group, the level of mouse IFN-γ protein in the tumor site increased significantly in the rNDV-mOX40L-treated group. Taken together, rNDV-mOX40L exhibited superior anti-tumor immunity by stimulating tumor-specific T cells and may be a promising agent for cancer immunotherapy.

Introduction

NDV is an avian paramyxovirus with a negative-sense single-stranded RNA genome and it has been a promising way for cancer therapy. Decades of researches have demonstrated the natural and selective oncolytic capabilities of NDV in different cancer cell lines. In the early 1950s, adenovirus and NDV were injected directly into uterine carcinoma, resulting in partial necrosis and sloughing, but followed by regrowth [1, 2]. This might be due to the production of neutralizing antibodies that inhibited the oncolytic activity of NDV [2]. After that, many reports showed the possibility of NDV as a therapeutic agent in cancer treatment [3, 4]. These advances have shifted the role of NDV from simply lysis of tumor cells to a strategy of inflaming treated tumors and the microenvironment, recruitment of immune cells, and inducing anti-tumor immune responses. Thus, the activation of the immune system is critical to developing long-term priming and memory targeted against malignant cells and enhancing the anti-tumor effect [5]. However, the clinical application of NDV is unsatisfactory, which may be due to the anti-tumor immunity of NDV is still limited. We speculated that the viral therapy coupled with immune costimulatory factors

✉ Wei Xiao
xw_kanion@163.com

✉ Deshan Li
deshanli@163.com

[1] College of Life Science, Northeast Agricultural University, Harbin, China

[2] Jiangsu Kanion Pharmaceutical CO. LTD, State Key Laboratory of New-tech for Chinese Medicine Pharmaceutical Process, Lianyungang, Jiangsu, China

[3] Present address: College of Life Science, Northeast Agricultural University, Harbin 150030 Heilongjiang, China

may further expand the therapeutic window of NDV, so it is necessary to conduct a study on the combination therapy of NDV.

Immune costimulatory factor, OX40L, is a member of the TNF superfamily. This superfamily also consists of CD70, 4-1BBL, and GITRL. OX40L is a 34 kDa glycosylated type II transmembrane protein trimer, typically presenting on the surface of antigen-presenting cells [6, 7], and its receptor OX40 is predominantly expressed on activated $CD4^+$ and $CD8^+$ T cells [8]. Early studies have revealed that OX40/OX40L interaction affects T cell expansion, survival, and cytokine production after OX40L delivers a potent costimulatory signal to activated $CD4^+$ and $CD8^+$ T cells. Moreover, the receptor of OX40L was upregulated on many immune cells upon activation [9, 10] and its agonist antibodies have shown therapeutic benefit in both preclinical cancer models and cancer patients [11, 12]. Preclinical cancer models have shown that anti-OX40 has potent anti-tumor activity against multiple tumor types, which is dependent on both $CD4^+$ and $CD8^+$ T cells [11, 13–15]. A Phase I clinical trial (#NCT01644968) in patients with melanoma showed that anti-OX40 increased proliferation of peripheral blood $CD4^+$ and $CD8^+$ T cells and endogenous tumor-specific immune responses [16]. Thus, activation of co-stimulation receptors may enhance anti-tumor immunity in cancer therapy.

In this study, we attempt to improve the anti-tumor immune response of NDV by modifying its genome, which expresses murine OX40L. The anti-tumor effects induced by rNDV-mOX40L were examined in the CT26 model. Compared to NDV, rNDV-mOX40L was more efficient to increase tumor-infiltrating T cells in the tumor site. Our data strongly indicated that rNDV-mOX40L is a promising agent for cancer immunotherapy.

Materials and method

Cell lines and cell cultures

The cell lines CT26, BHK-21, and DF-1 were reserved by Biopharmaceutical Laboratory of Northeast Agricultural University. CT26 cells were maintained in RPMI 1640 medium (with 10% fetal bovine serum and 1% penicillin /streptomycin) at 37 °C with 5% CO_2 and 100% humidity. DF-1 and BHK-21 cells were cultured in DMEM (with 10% fetal bovine serum and 1% penicillin/streptomycin) at 37 °C with 5% CO_2 and 100% humidity.

Viruses

The original framework of the NDV strain is the lentogenic strain rClone30. Furthermore, in order to improve the oncolytic effect of the virus, the recombinant plasmid pNDV was constructed by exchanging the F gene of lentogenic strain rClone30 with velogenic strain F48E9, and then the chimeric virus rNDV was constructed [17]. The plasmid *pNDV* was obtained from the Biopharmaceutical Laboratory of Northeast Agricultural University and served as the backbone for the modification of the NDV genome. Murine OX40L can stimulate both human and mouse T cells, however, human OX40L can only stimulate human T cells [18]. Thus, we select murine *OX40L* gene to construct recombinant NDV. The gene of the extracellular domain (aa 49–198) of *mOX40L* was obtained from Genbank (U12763). Plasmid *pPUC-mOX40L* containing *mOX40L* gene was purchased from Sangon Biotech. The *mOX40L* gene was cloned into the *Sac*II and *Pme*I cloning site in between the P and M genes. The resulting plasmid was named *prNDV-mOX40L*. Recombinant NDV were then rescued by transfecting BHK-21 cells with *prNDV-mOX40L* (2 μg) along with the helper plasmids *pTM-NP* (1 μg), *pTM-P* (0.5 μg), *pTM-L* (0.25 μg). The culture supernatant was harvested at 72 h post transfection and inoculated into 9-day-old-specific pathogen-free (SPF) embryonated chicken eggs, and viral titers were determined by hemagglutination assay.

Growth kinetics of the viruses

The growth curve of the recombinant NDV was determined by a growth assay in CT26 cells. CT26 cells were plated at 1×10^6 cells/well and were infected the next day with a virus at 0.01 MOI, the cells were kept in a 37 °C humidified incubator equipped with 5% CO_2. Cells supernatant were collected and frozen at 12, 24, 36, 48, 60, and 72 h after infection. The virus (100 μL) of tenfold serial dilutions in RPMI 1640 were added to plates containing 5×10^4 cells/well. The viral concentration was measured by end-point titration in CT26 cells and calculated as 50% tissue culture infective dose ($\log_{10}TCID_{50}$) per milliliter.

Mice

Female BALB/c mice (6–8 weeks old) were purchased from Comparative medicine of Yangzhou University. Animal care and experimental procedures were performed under SPF conditions. All animal protocols were followed by National Institute of Health and the Institutional Animal Care and Use Committee of Northeast Agriculture University. Mice were injected subcutaneously with 1×10^5 CT26 cells on the right flank. When tumor size reached 5–8 mm in diameter (5–7 days), the mice were intratumorally inoculated with NDV (100 μL of 10^7 PFU), rNDV-mOX40L (100 μL of 10^7 PFU), and PBS (100 μL) every day for a total of 14 injections. Mice were randomly divided

into three groups ($n = 6$). The tumor sizes were monitored every other day. Animals were sacrificed when tumor size reached 15 mm in any dimension or at the termination of the experiment. The tumor volume was calculated using the following formula: tumor volume (mm^3) = [(width)^2 × length]/2. The inhibition rate was calculated using the following formula: tumor inhibition rate (%) = (1 − tumor volume of treated-group/tumor volume of model group) × 100%. The tumors were placed in 4% formalin for further histological analysis.

Western blot

A total of 1×10^5 CT26 cells were plated per well in a six-well plate and infected with rNDV-mOX40L and NDV (as the control) at 1 MOI after growing to 70–80% confluence. After 24 h post infection, the supernatants were harvested. For tumor tissues, three tumor tissues were selected from each group. In each group, tumor tissue was homogenized in RIPA lysis buffer supplemented with 1 mM PMSF for 30 min. After full lysis, centrifugation was performed at 12,000 rpm at 4 °C for 10 min. The supernatant was taken for western blot. For western blotting analysis, equivalent amounts of whole samples were separated by SDS-PAGE, and transferred to a nitrocellulose membrane. The membrane was incubated in blocking buffer at room temperature for 10 min, incubated in primary antibody buffer at 4 °C overnight, and incubated in horseradish peroxidase-conjugated secondary antibody buffer at room temperature for 1 h. Protein bands were detected with the ECL system (Thermo Fischer) and a gel imaging system (ChemiDocTM XRS+, Bio-Rad, USA) according to the manufacturer's recommendations. Primary antibody included anti-OX40L (ab156285; Abcam) and anti-IFN-γ (AMC4739; Thermo Fischer).

Flow cytometry analysis (FACS)

The spleens from the sacrificed mice were dissociated into a single-cell suspension. Cells were then stained with PE anti-mouse $CD4^+$ (LS-C62735; LSBio), APC anti-mouse $CD8^+$ (17-0081-82; Thermo Fisher), and FITC anti-mouse $CD3^+$ (ab239226; Abcam) for 2 h at room temperature. After washing twice with PBS and resuspending in PBS, the stained cells were analyzed by Becton Dickinson FACS flow cytometer.

Immunohistochemistry and histopathology

Tumor tissues from tumor-bearing mice were fixed in 4% formalin at room temperature for 48 h, processed through graded concentrations of ethanol and xylene, and embedded in paraffin wax. The H&E histopathology staining was carried out according to the protocol described by Cardiff et al. For immunohistochemistry, slides were incubated with anti-CD4 (ab237722; Abcam), anti-CD8 (ab217344; Abcam) antibody, and anti-OX40 (ab229021; Abcam) at 4 °C overnight and incubated within horseradish peroxidase-conjugated secondary antibody. The scoring assessment of immunolabeling for CD4, CD8, and OX40 was detected by ImageJ [19].

CCK-8 assay

CCK-8 assay was used to quantify cell viability. A total of 1×10^4 cells were plated per well in a 96-well plate and incubated with virus at 0.01, 0.1, 1 and 10 MOI. Ten microliters CCK-8 solution (BestBio, BB-4202–3;1000T) was added to the cells at 24, 48, and 72 h after infection. A spectrophotometer was used to determine the optical density (OD) at the absorbance of 450 nm after 4 h incubation, all samples were detected in triplicates. Cytotoxicity was quantified as the difference in cell viability between the experimental samples and the uninfected controls. The cell viability was converted and expressed using the formula:

$$\text{Inhibition ratio} = (\text{control group OD} - \text{treatment group OD})/\text{control group OD} \times 100\%$$

Statistical analysis

The results were analyzed using GraphPad Prism 7.0 software. The results were expressed as mean ± standard deviation. Statistically significant differences were determined by Student's paired two-tailed t test. $^*P < 0.05$ was considered statistically significantly.

Results

Generation and growth curve of rNDV-mOX40L

Following the previous description, reverse-genetics technology was used for the construction of NDV [20, 21]. As shown in Fig. 1A, *mOX40L* gene was sub-cloned into the NDV genome between P and M gene. The RT-PCR and sequencing confirmed that the location and orientation of the inserted *mOX40L* gene were correct.

The growth characteristics of rNDV-mOX40L and NDV were determined in CT26 cells to assess the effect of foreign gene *mOX40L* on viral growth. CT26 cells were infected with 0.01 MOI viruses and the supernatant of them was harvested at different time to determine the viral titers. As shown in Fig. 1B, the statistical data demonstrated that there was no significant difference between NDV and rNDV-mOX40L in replication kinetics, indicating that the

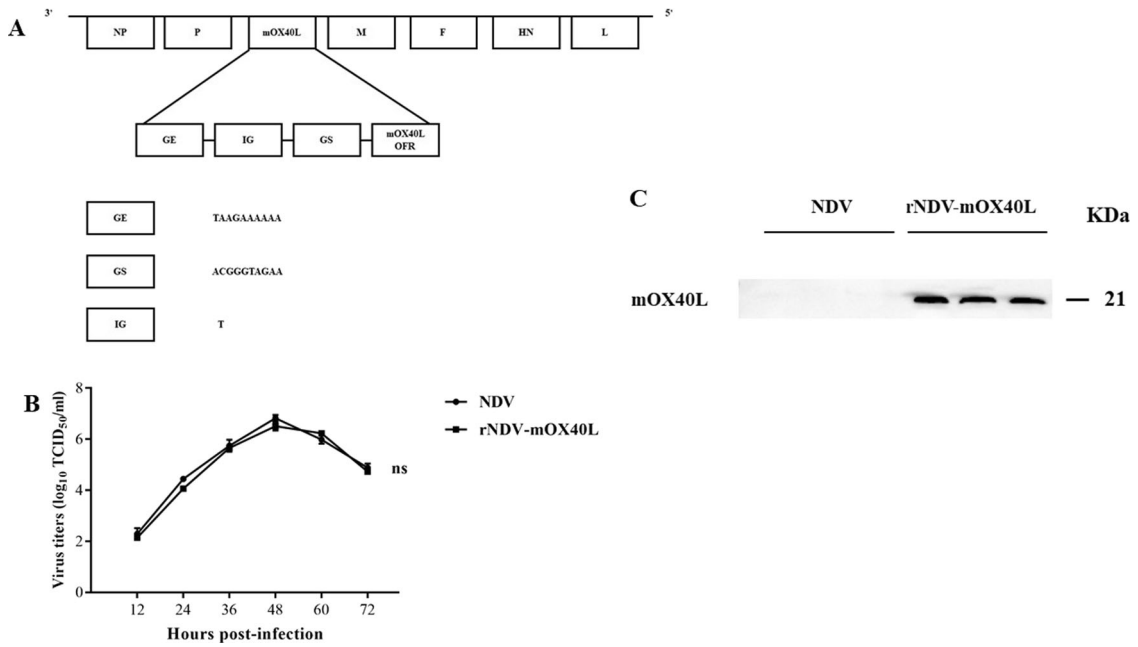

Fig. 1 Construction and growth curve of rNDV-mOX40L. A Schematic representation of rNDV-mOX40L. The coding sequence mOX40L was inserted into the NDV genome at the position between P and M gene. The GS (gene-start) and GE (gene-end) sequences were introduced before the ORF (open reading frame) of the mOX40L gene. IG: intergenic region. **B** Growth kinetics of rNDV-mOX40L and NDV in CT26 cells, CT26 cells were infected with 0.01 MOI viruses. The virus titers were determined by $TCID_{50}$ in CT26 cells at 12, 24, 36, 48, 60, and 72 h post infection. **C** Expression of mOX40L protein in vitro. In vitro, CT26 cells were infected with rNDV-mOX40L and NDV (as the control) at 1 MOI after the cells growing to 70–80% confluence. After 24 h post infection, cell supernatant was harvested for western blot. Values represent mean ± SD of triplicate samples.

insertion of *mOX40L* gene does not affect the growth kinetics of NDV.

To test the expression of mOX40L protein in vitro, CT26 cells infected with viruses were assessed by western blot. The cell supernatant infected with rNDV-mOX40L or NDV (as the control) at 24 h post infection was harvested and assayed using western blot. A band of ~21 kDa, corresponding to the molecular weight of murine OX40L protein was detected in the cell supernatant infected with rNDV-mOX40L, but not in the cell supernatant infected with NDV (Fig. 1C). Overall, these results indicate that rNDV-mOX40L expresses high level of mOX40L protein in vitro.

In vitro cytotoxicity evaluation of rNDV-mOX40L

To better characterize the rNDV-mOX40L virus in comparison to the parental virus NDV, the cytotoxic activities of NDV and rNDV-mOX40L were tested in CT26 cells at different time points (24, 48, 72 h) post infection by CCK-8 assay. As shown in Fig. 2, The growth inhibition rates of NDV-treated group and rNDV-mOX40L-treated group increased along with time. The growth inhibition rates of NDV-treated group at 0.01, 0.1, 1, 10 MOI were 38.087%, 48.6493%, 55.1386%, 75.67535% respectively at 72 h post infection. And, the growth inhibition rates of rNDV-mOX40L-treated group at 0.01, 0.1, 1, 10 MOI were 37.9707%, 47.9206%, 53.90765%, 74.4259% respectively at 72 h post infection. The statistical data demonstrated that there is no significant difference between NDV and rNDV-mOX40L in cytotoxic activity.

Furthermore, CT26 cells were infected with viruses at MOI of 1 and the representative photomicrographs at different time points (0, 24, 48, 72 h) post infection were recorded. The CT26 cells in both the NDV-treated group and the rNDV-mOX40L-treated group showed cellular volume small, loose between the cells and adherent ability decreased compared with those in the untreated group at 24 h post infection. The CT26 cells in both the NDV-treated group and the rNDV-mOX40L-treated group appeared swelling, roundness, and syncytium at 48 h post infection. The CT26 cells in both NDV-treated group and rNDV-mOX40L-treated group appeared cells death and fragments at 72 h post infection (Fig. 2E).

rNDV-mOX40L significantly inhibits the growth of tumor in the CT26 model

In order to explore the anti-tumor effect of rNDV-mOX40L in vivo, CT26 model was constructed to detect the oncolytic activity of rNDV-mOX40L. On day 14 after administration, mice were sacrificed for further analysis. As shown in Fig. 3A, the tumor size of the animals in the NDV or

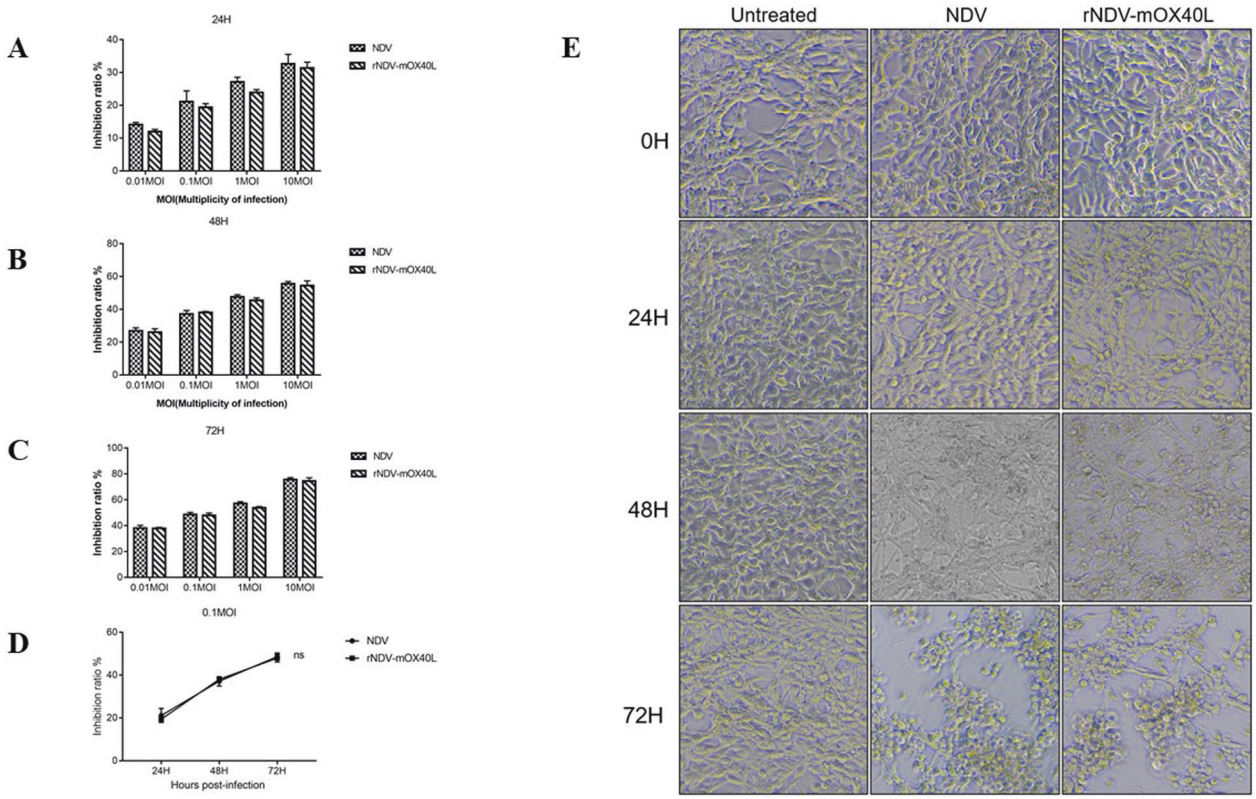

Fig. 2 In vitro cytotoxicity evaluation of rNDV-mOX40L. 1×10^4 cells of 100 µL were plated per well in a 96-well plate and incubated with virus at 0.01, 0.1, 1, and 10 MOI. **A**–**C** The cytotoxic activities of NDV and rNDV-mOX40L were tested in CT26 cells at different time points (24, 48, 72 h) after infection by a CCK-8 assay. **D** The cytotoxic activities of NDV and rNDV-mOX40L were tested in CT26 cells at MOI of 0.1 at different time points (24, 48, 72 h) by a CCK-8 assay. **E** The representative photomicrographs were recorded under the microscope at 0, 24, 48, and 72 h post infection. Values represent mean ± SD of triplicate samples. Student's paired two-tailed *t* test. ns: not significant.

rNDV-mOX40L-treated groups was smaller than that in the PBS-treated group. As shown in Fig. 3B, the average volume of the PBS-treated group was 1408.15 mm^3, the average volume of the NDV-treated group was 355.33 mm^3 and the average volume of the rNDV-mOX40L-treated group was 163.36 mm^3. The tumor volume of rNDV-mOX40L-treated group was significantly suppressed compared with that of the NDV-treated group or PBS-treated group. As shown in Fig. 3C, the tumor inhibition rates of the NDV-treated group and the rNDV-mOX40L-treated group were 66.26% and 81.44%, respectively. Overall, these results suggest that rNDV-mOX40L significantly inhibits the growth of tumor in the CT26 model.

rNDV-mOX40L expresses high levels of mOX40L protein in vivo

In vivo, tumor tissues were selected from each group and assayed using western blot. As shown in Fig. 4A, the expression of mOX40L protein in the tumor tissues of rNDV-mOX40L-treated group was significantly higher than that in NDV-treated group and PBS-treated group. Furthermore, immunohistochemistry staining also confirmed this result (Table 1). Overall, these results indicate that rNDV-mOX40L expresses high level of mOX40L protein in vivo.

rNDV-mOX40L induces tumor necrosis and tumor-infiltrating lymphocytes in the CT26 model

To test the anti-tumor immunity of rNDV-mOX40L, tumors were excised on day 14 post administration, and the morphological changes in tumors were assessed by H&E. Then these tumor tissues were stained with anti-CD4 and anti-CD8 antibody, the lymphocytes infiltration was analyzed by immunohistochemistry staining. As shown in Fig. 5A, the tumor cells of PBS-treated group were arranged tightly, having a large nucleus and obvious nucleoli. The tumor cells of NDV-treated group appeared nuclear pyknosis, showing a relatively narrow tumor region. While, the tumor cells of rNDV-mOX40L-treated group exerted a loose arrangement and a large necrotic region. In addition, the tumor cells of the rNDV-mOX40L-treated group showed nuclear deformation, nuclear pyknosis, the disappearance of nucleoli, unclear nuclear structure, and nuclear disaggregation. As shown in

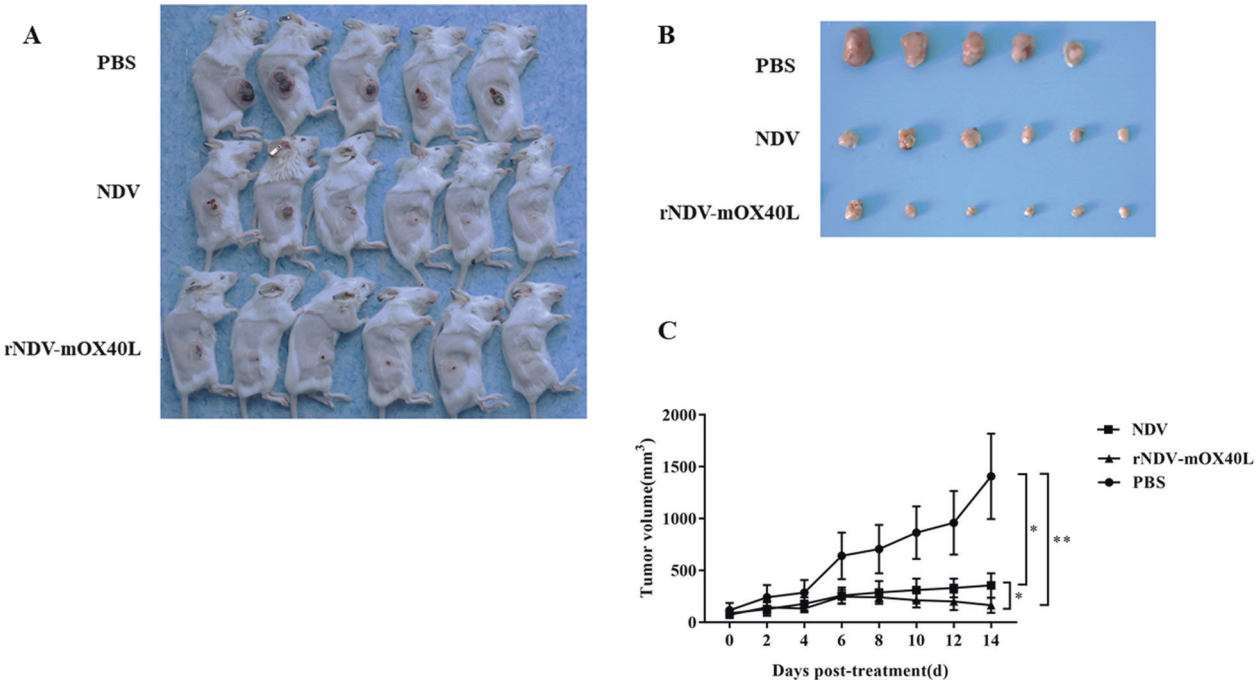

Fig. 3 rNDV-mOX40L show enhanced oncolytic effect in CT26 model. Six-week-old female BALB/c mice were injected in the right groin with 1×10^6 CT26 cells and mice were randomly divided into three groups and intratumorally injected with 10^7 pfu virus every day for a total of fourteen times. On day 14 after administration, the mice were sacrificed for further analysis. **A** The tumor in the right groin of different groups of mice before necropsy. During treatment, one mouse of the PBS-treated group died on day 8 for unknown reasons. **B** The tumor tissues of PBS, NDV, and rNDV-mOX40L-treated group. **C** The tumor growth curve of CT26-bearing mice from day 0 to day 14 of treatments. Values represent mean ± SD of triplicate samples. $n = 6$; Student's paired two-tailed t test. $^*p < 0.05$; $^{**}p < 0.01$, compared with the NDV-treated group.

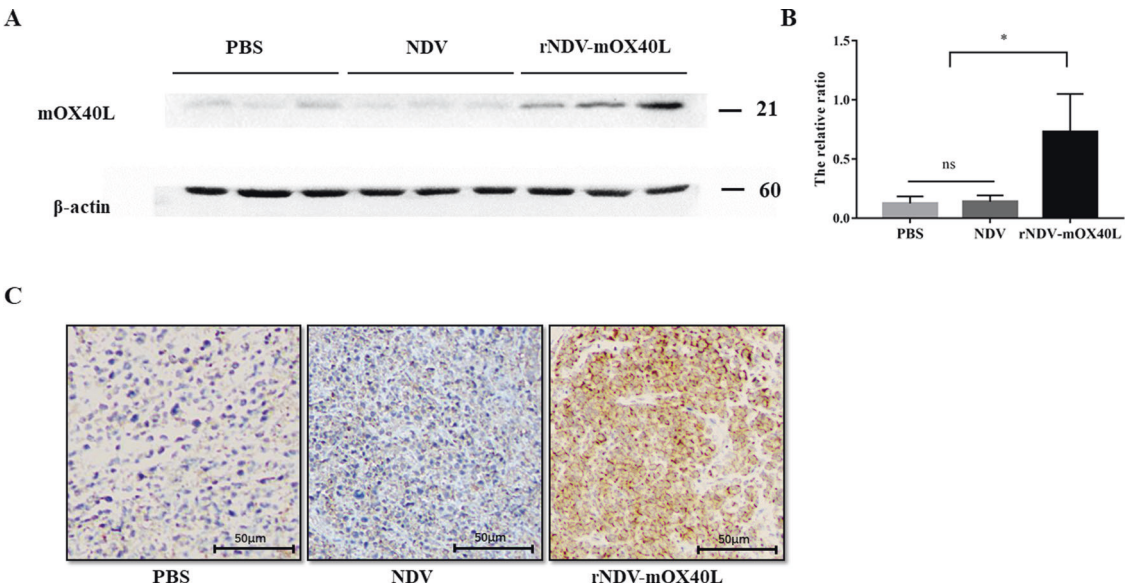

Fig. 4 Expression of mOX40L protein in vivo. A In vivo, the expression of mOX40L protein in the tumor tissues from the sacrificed mice was detected by western blot. $n = 3$. **B** The relative ratio between mOX40L and β-actin proteins in tumor tissues. **C** Immunochemical staining for mOX40L protein of tumor tissues from CT26-bearing mice (×200 magnification). $n = 3$. The immunohistochemistry data were performed from consecutive sections. The expression of mOX40L protein was shown in brown. The NDV-treated group as the control group. Values represent mean ± SD of triplicate samples. Student's paired two-tailed t-test. ns: not significant ($p \geq 0.05$); $^*p < 0.05$, compared with the NDV-treated group (color figure online).

Table 1 The scoring assessment of immunolabeling for OX40L.

Antibody	PBS	NDV	rNDV-mOX40L
OX40L	−	−	++

Fig. 5B, C, the immunohistochemistry staining pattern of the rNDV-mOX40L-treated group exhibited more tumor-infiltrating $CD4^+$ and $CD8^+$ T lymphocytes compared with the NDV-treated group and PBS-treated group in the CT26

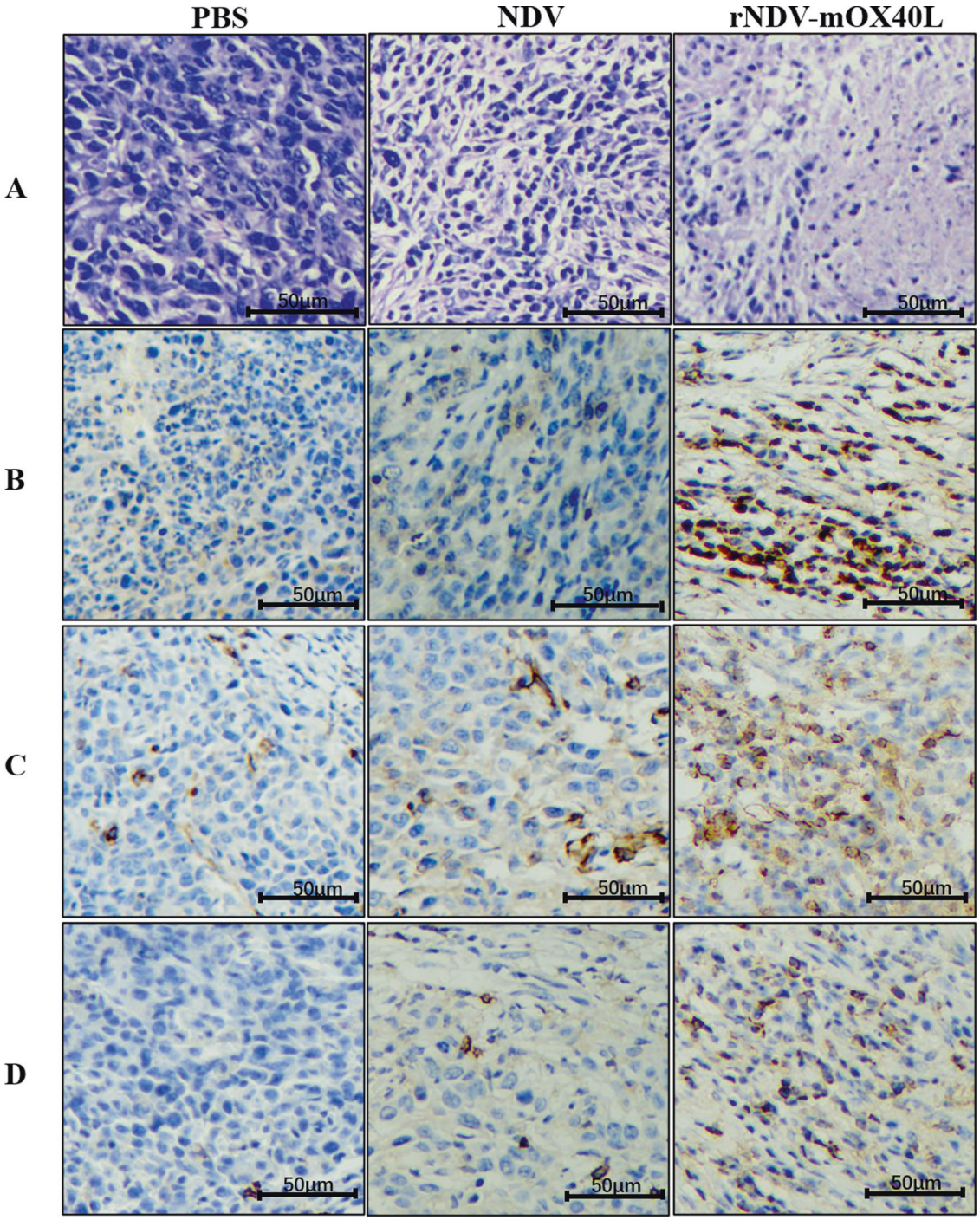

Fig. 5 H&E and immunohistochemistry staining of tumor tissues in CT26 model. The morphological changes and lymphocytes infiltration in the tumor tissues from the sacrificed mice were analyzed by H&E and immunohistochemistry staining. The immunohistochemistry data were performed from consecutive sections. **A** Representative sections of H&E-stained mouse tumors (×200 magnification). **B** Immunochemistry staining for $CD4^+$ T cells of tumor tissues (×200 magnification). **C** Immunochemistry staining for $CD8^+$ T cells of tumor tissues (×200 magnification). **D** Immunochemistry staining for $OX40^+$ T cells of tumor regions rich in $CD4^+$ and $CD8^+$ T cells (×200 magnification). The NDV-treated group as the control group. $n = 3$. Values represent mean ± SD of triplicate samples.

model. These results suggest that rNDV-mOX40L promotes anti-tumor responses by increasing necrosis and T-cell infiltrations in tumors.

To examine the T cells activation marker OX40 in the tumor site, tumor tissues were stained with anti-OX40 antibody (Fig. 5D) in above areas rich in $CD4^+$ and $CD8^+$ T cells. Immunohistochemical findings are summarized in Table 2, the result showed that the immunohistochemistry staining pattern of the rNDV-mOX40L-treated group exhibited more $OX40^+$ T cells infiltration compared with that of NDV-treated group and PBS-treated group in the CT26 model, suggesting that rNDV-mOX40L promotes anti-tumor responses by increasing $OX40^+$ T cells infiltration in the tumor.

Table 2 The scoring assessment of immunolabeling for CD4, CD8, and OX40.

Antibody	PBS	NDV	rNDV-mOX40L
CD4	−	+	+++
CD8	−	+	++
OX40	−	+	++

rNDV-mOX40L stimulates splenic lymphocytosis

To further study the immune responses induced by rNDV-mOX40L, FACS was used to analyze the percentages of $CD3^+$, $CD4^+$ and $CD8^+$ T cells in the spleen of mice. As shown in Fig. 6B, the percentages of $CD4^+$ T cells in the control group, PBS-treated group, NDV-treated group and rNDV-mOX40L-treated group were 25.9%, 11.16%, 13.16%, and 24.16%, respectively. While the percentages of $CD8^+$T cells in control group, PBS-treated group, NDV-treated group and rNDV-mOX40L-treated group were 17.47%, 8.3%, 8.73% and 16.7%, respectively. There was no significant difference in the percentage of $CD4^+$ T cells and $CD8^+$ T cells between the control group and rNDV-mOX40L-treated group. However, the percentages of $CD4^+$ T cells and $CD8^+$ T cells in rNDV-mOX40L-treated group were significantly higher than that in NDV-treated group and PBS-treated group, suggesting that

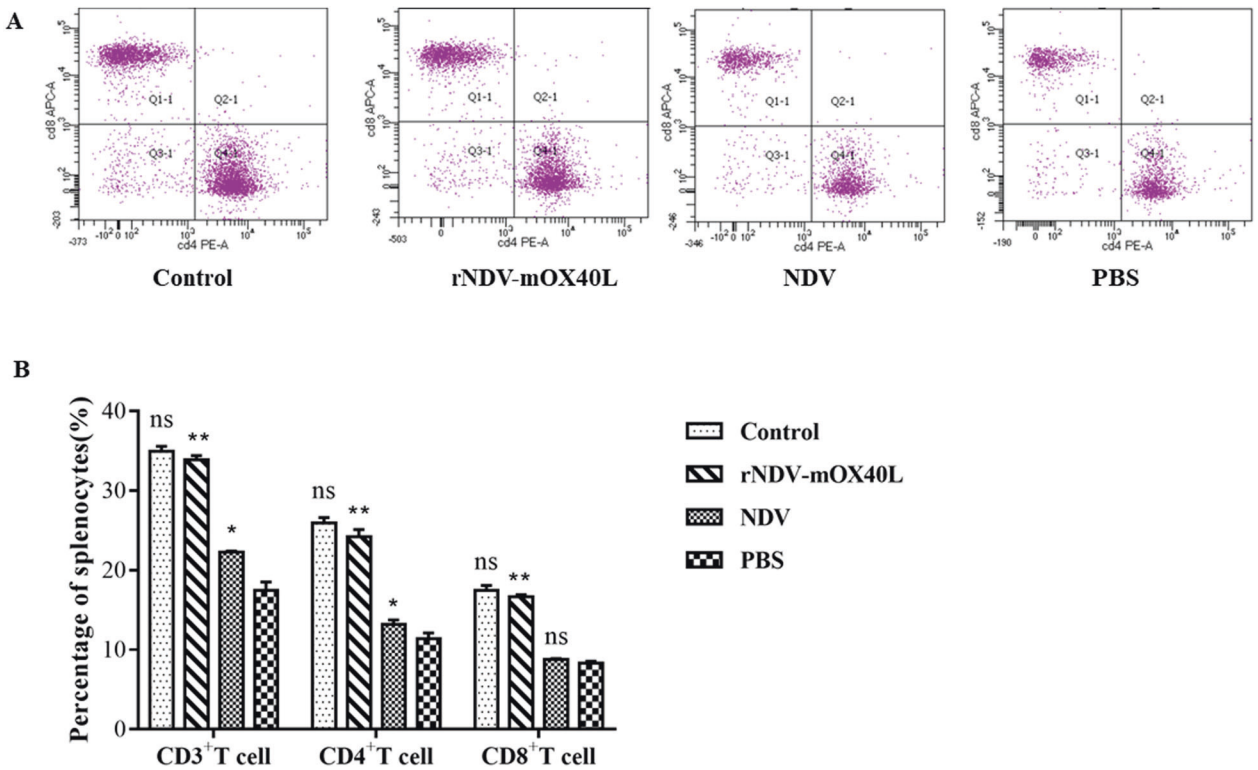

Fig. 6 Enhancement of splenic immune response induced by rNDV-mOX40L. The spleens from the sacrificed mice were dissociated into single-cell suspension. The splenocytes were analyzed for the percentages of $CD3^+$, $CD4^+$ and $CD8^+$ T cells by FACS. **A** Scatter plots of $CD4^+$ and $CD8^+$ T cells in the spleen. The *X* axis represents $CD4^+$—PE and the *Y* axis represents $CD8^+$—APC. **B** The percentages of $CD3^+$, $CD4^+$ and $CD8^+$ T cells in the spleen. The mice in the control group were normal healthy mice, and the control group is a positive control. $CD3^+$ T cells and $CD4^+$ T cells: ns (control vs rNDV-mOX40L); $^{**}p < 0.01$ (rNDV-mOX40L vs NDV or PBS); $^{*}p < 0.05$ (NDV vs PBS); $CD8^+$ T cells: ns (control vs rNDV-mOX40L; NDV vs PBS); $^{**}p < 0.01$ (rNDV-mOX40L vs NDV or PBS); $n = 3$. Values represent mean ± SD of triplicate samples. Student's paired two-tailed *t* test. ns not significant ($p \geq 0.05$); $^{**}p < 0.01$; $^{*}p < 0.05$.

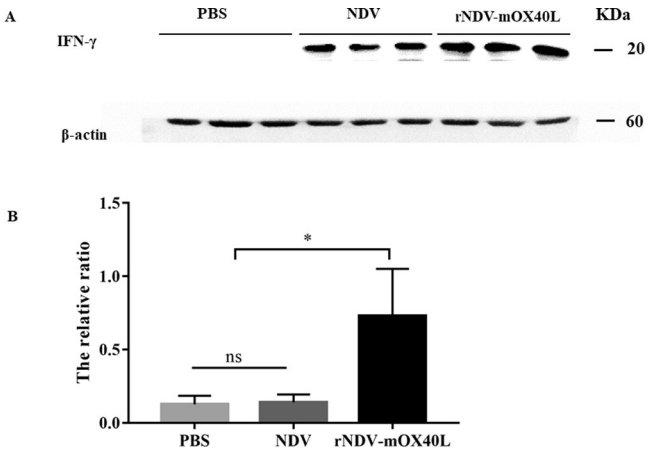

Fig. 7 The rNDV-mOX40L promotes IFN-γ production in tumor tissues. A The tumor tissues from the sacrificed mice were assessed for the IFN-γ secretion by western blot. A band of ~20 kDa was detected from tumor tissues of three groups. **B** The relative ratio between IFN-γ and β-actin proteins in tumor tissues. $n = 3$. Values represent mean ± SD of triplicate samples. Student's paired two-tailed t test. ns: not significant ($p \geq 0.05$); *$p < 0.05$.

rNDV-mOX40L promotes anti-tumor response by stimulating splenic T cell response.

rNDV-mOX40L stimulates the expression of IFN-γ protein in the tumor tissue

Engagement of OX40 by OX40L stimulates T-cell activity in humans and mice [22]. To examine the expression of IFN-γ protein induced by rNDV-mOX40L in the tumor tissue, tumor tissues were excised on day 14. Then, the IFN-γ protein was assessed by western blot. As shown in Fig. 7A, a band of ~20 kDa, corresponding to the molecular weight of mouse IFN-γ protein, was detected from tumor tissues of three groups. The IFN-γ protein level of the rNDV-mOX40L-treated group was significantly higher than that of the NDV-treated group and PBS-treated group, indicating that rNDV-mOX40L promotes anti-tumor response by upregulated the protein level of IFN-γ in the tumor tissues.

Discussion

Clinical experience has shown that the antiviral immune response and limited anti-tumor immunity constrain the oncolytic effect of the viruses. To improve the therapeutic efficiency of NDV, the viruses have been modified to express cytokines or combined with immune checkpoint inhibitors [22]. Herpes simplex virus expressed GM-CSF (T-Vec) has shown enhanced efficacy in melanoma patients [23]. Recombinant NDV Anhinga strain expressed IL-2 effectively inhibits the growth of hepatocellular carcinoma in vivo [24]. Previous studies have shown that OX40L binds a unique co-stimulator OX40 on T cells [12–14], making it a better choice to arm the virus to enhance activation of T cells recognizing tumor antigens on tumor cells infected by the virus. In this study, we engineered recombinant NDV to express immune co-stimulator OX40L, recruiting and enhancing T-cell activation in tumors. Then, the anti-tumor immune response induced by rNDV-mOX40L is more localized to cancer cells.

To better characterize the rNDV-mOX40L virus in comparison to the parental virus, the virus replication kinetics, the number of syncytia, and the inhibition rate of the two viruses on CT26 cells were determined. The result showed that there was no significant difference between NDV and rNDV-mOX40L, indicating that the insertion of mOX40L gene does not affect the replication rate and syncytium-inducing capacity of NDV in vitro (Figs. 1B and 2).

The CT26 tumor model was used next to assess the ability of the recombinant viruses to induce anti-tumor effect. The tumor volume of CT26 tumor-bearing mice was significantly inhibited by rNDV-mOX40L (Fig. 3C). The tumor inhibition rate of rNDV-mOX40L-treated group was 81.44%. The tumor inhibition rate of the rNDV-mOX40L-treated group was increased by 15.18% compared to the NDV-treated group. H&E analysis showed increased tumor necrosis in the rNDV-mOX40L-treated group compared with that in the NDV-treated group. In vivo engagement of rNDV-mOX40L resulted in a significant therapeutic benefit in the CT26 model.

T cells have a central role in supporting and shaping immune responses and have a key role in anti-tumor immunity. It is now clear that elevated levels of tumor-infiltrating T cells as well as a systemic anti-tumor immune response are requirements for successful immunotherapies. The increased percentages of $CD4^+$ and $CD8^+$ tumor-infiltrating T cells is often correlated with improved clinical outcome in several cancers. Moreover, Weinberg [13] reported that OX40 may expand tumor-reactive T cells by $OX40^+$ T cells in vivo. T cells traffic to areas where their target antigens are expressed and can produce cytokines and chemokines that affect tumor growth. $CD4^+$ T cells are

capable of activating and regulating many aspects of innate and adaptive immunity, including the function of cytotoxic $CD8^+$ T cells [25]. Major CTL activities are mediated either directly, through synaptic exocytosis of cytotoxic granules containing perforin and granzymes into the target, resulting in cancer cell destruction, or indirectly, through secretion of cytokines, including interferon (IFN-γ) and tumor necrosis factor (TNF) [26, 27].

To study the effects of rNDV-mOX40L on the expression and function of T cells in vivo, splenocytes and tumor tissues isolated from tumor-bearing mice were analyzed by immunohistochemistry staining and flow cytometry. The more $CD4^+$ and $CD8^+$ T cells were found in the splenocytes isolated from tumor-bearing mice treated with rNDV-mOX40L (Fig. 6B). The infiltration of tumor-infiltrating $CD4^+$, $CD8^+$ and $OX40^+$ T lymphocytes were increased in the rNDV-mOX40L-treated group compared with that in NDV and PBS-treated group (Fig. 5B–D). In addition, the level of IFN-γ were also upregulated after the mice were treated by rNDV-mOX40L, suggesting that rNDV-mOX40L induces CTL activities of T cells (Fig. 7). These results suggest that rNDV-mOX40L enhances the systemic and tumor-specific anti-tumor immunity by the costimulatory signal of mOX40L.

In conclusion, rNDV-mOX40L showed a better anticancer efficacy than its predecessor NDV in the CT26 model, augmenting a local and systemic response to cancer. Based on the anti-tumor properties of rNDV-mOX40L, this recombinant virus has the potential for clinical application in patients with colorectal cancer.

Acknowledgements This work was financially supported by the National Key R&D Program of China (2017YFD0501102).

Author contributions LT: conceptualization, methodology, validation, formal analysis, investigation, writing-original draft, visualization. DL: conceptualization, methodology, validation, supervision, resources, data curation. WX: methodology, project administration, funding acquisition, data curation. TL: validation, methodology, investigation. YC: validation, investigation. SJ: validation, software. HS: validation, investigation. KK: validation, investigation. ZW: project administration, funding acquisition. GR: methodology, resources.

Compliance with ethical standards

Conflict of interest The authors declare no competing interests.

Publisher's note Springer Nature remains neutral with regard to jurisdictional claims in published maps and institutional affiliations.

References

1. Cassel WA, Garrett RE. Newcastle disease virus as an antineoplastic agent. Cancer. 1965;18:863–8.
2. Lam HY, Yeap SK, Pirozyan MR, Omar AR, Yusoff K, Suraini AA, et al. Safety and clinical usage of Newcastle disease virus in cancer therapy. J Biomed Biotechnol. 2011;2011:718710.
3. Omar AR, Ideris A, Ali AM, Othman F, Yusoff K, Abdullah JM, et al. An overview on the development of newcastle disease virus as an anti-cancer therapy. Malays J Med Sci. 2003;10:4–12.
4. Csatary SE LK, Bukosza I. Attenuated veterinary virus vaccine for the treatment of cancer. Cancer Detect Prev. 1993;17:619–27.
5. McCormack RM, Kaur B. Immune therapy, a double-edged sword for oncolytic viruses. Expert Opin Biol Ther. 2019;19:1111–3.
6. Fu Y, Lin Q, Zhang Z, Zhang L. Therapeutic strategies for the costimulatory molecule OX40 in T-cell-mediated immunity. Acta Pharm Sin B. 2020;10:414–33.
7. Sanmamed MF, Pastor F, Rodriguez A, Perez-Gracia JL, Rodriguez-Ruiz ME, Jure-Kunkel M, et al. Agonists of co-stimulation in cancer immunotherapy directed against CD137, OX40, GITR, CD27, CD28, and ICOS. Semin Oncol. 2015;42:640–55.
8. Ishii N, Takahashi T, Soroosh P, Sugamura K. OX40-OX40 ligand interaction in T-cell-mediated immunity and immunopathology. Adv Immunol. 2010;105:63–98.
9. Croft M. Control of immunity by the TNFR-related molecule OX40 (CD134). Annu Rev Immunol. 2010;28:57–78.
10. Schaer DA, Murphy JT, Wolchok JD. Modulation of GITR for cancer immunotherapy. Curr Opin Immunol. 2012;24:217–24.
11. Kjaergaard J, Tanaka J, Kim JA, Rothchild K, Weinberg A, Shu S. Therapeutic efficacy of OX-40 receptor antibody depends on tumor immunogenicity and anatomic site of tumor growth. Cancer Res. 2000;60:5514–21.
12. Moran AE, Kovacsovics-Bankowski M, Weinberg AD. The TNFRs OX40, 4-1BB, and CD40 as targets for cancer immunotherapy. Curr Opin Immunol. 2013;25:230–7.
13. Weinberg AD, Rivera MM, Prell R, Morris A, Ramstad T, Vetto JT, et al. Engagement of the OX-40 receptor in vivo enhances antitumor immunity. J Immunol. 2000;164:2160–9.
14. Gough MJ, Ruby CE, Redmond WL, Dhungel B, Brown A, Weinberg AD. OX40 agonist therapy enhances CD8 infiltration and decreases immune suppression in the tumor. Cancer Res. 2008;68:5206–15.
15. Piconese S, Valzasina B, Colombo MP. OX40 triggering blocks suppression by regulatory T cells and facilitates tumor rejection. J Exp Med. 2008;205:825–39.
16. Curti BD, Kovacsovics-Bankowski M, Morris N, Walker E, Chisholm L, Floyd K, et al. OX40 is a potent immune-stimulating target in late-stage cancer patients. Cancer Res. 2013;73:7189–98.
17. Wakamatsu N, King DJ, Seal BS, Samal SK, Brown CC. The pathogenesis of Newcastle disease: a comparison of selected Newcastle disease virus wild-type strains and their infectious clones. Virology. 2006;353:333–43.
18. Baum PR, Gayle RB, Ramsdell F, Srinivasan S, Sorensen RA, Watson ML, et al. Molecular characterization of murine and human OX40/OX40 ligand systems: identification of a human OX40 ligand as the HTLV-1-regulated protein gp34. EMBO J. 1994;13:3992–4001.
19. Jensen EC. Quantitative analysis of histological staining and fluorescence using ImageJ. Anat Rec. 2013;296:378–81.
20. Cardiff RD, Miller CH, Munn RJ. Manual hematoxylin and eosin staining of mouse tissue sections. Cold Spring Harb Protoc. 2014;2014:655–8.
21. Vigil A, Park MS, Martinez O, Chua MA, Xiao S, Cros JF, et al. Use of reverse genetics to enhance the oncolytic properties of Newcastle disease virus. Cancer Res. 2007;67:8285–92.
22. Sheridan C. First oncolytic virus edges towards approval in surprise vote. Nat Biotechnol. 2015;33:569–70.

23. Andtbacka RH, Kaufman HL, Collichio F, Amatruda T, Senzer N, Chesney J, et al. Talimogene Laherparepvec Improves Durable Response Rate in Patients With Advanced Melanoma. J Clin Oncol. 2015;33:2780–8.
24. Wu Y, He J, An Y, Wang X, Liu Y, Yan S, et al. Recombinant Newcastle disease virus (NDV/Anh-IL-2) expressing human IL-2 as a potential candidate for suppresses growth of hepatoma therapy. J Pharmacol Sci. 2016;132:24–30.
25. Hung K, Hayashi R, Lafond-Walker A, Lowenstein C, Pardoll D, Levitsky H. The central role of CD4(+) T cells in the antitumor immune response. J Exp Med. 1998;188:2357–68.
26. Waldmann TA. Cytokines in cancer immunotherapy. Cold Spring Harb Perspect Biol. 2018;10:a028472.
27. Durgeau A, Virk Y, Corgnac S, Mami-Chouaib F. Recent advances in targeting CD8 T-cell immunity for more effective cancer immunotherapy. Front Immunol. 2018;9:14.